Efficient Tumor and Mitochondria Uptake of ^{177}Lu-Porphyrin-PEG Nanocomplexes for Multimodal Imaging Guided Combination Therapy

Dr. Bo Yu[a],[b],[c], **Dr. Hao Wei**[d], **Prof. Qianjun He**[a], **Carolina A. Ferreira**[b], **Christopher J. Kutyreff**[b], **Dr. Dalong Ni**[b], **Zachary T. Rosenkrans**[e], **Prof. Liang Cheng**[f], **Prof. Faquan Yu**[c], **Prof. Jonathan W. Engle**[b], **Prof. Xiaoli Lan**[d], and **Prof. Weibo Cai**[b],[e],[g]

[a]National-Regional Key Technology Engineering Laboratory for Medical Ultrasound, Guangdong Key Laboratory for Biomedical Measurements and Ultrasound Imaging, School of Biomedical Engineering, Health Science Center, Shenzhen University, Shenzhen 518060, China

[b]Departments of Radiology and Medical Physics. University of Wisconsin - Madison, USA 53705

[c]Key Laboratory for Green Chemical Process of Ministry of Education, School of Chemical Engineering and Pharmacy, Wuhan Institute of Technology, Wuhan 430022, China

[d]Dept of Nuclear Medicine, Union Hospital, Tongji Medical College, Huazhong University of Science and Technology, Wuhan 430073, China

[e]School of Pharmacy, University of Wisconsin - Madison, USA 53705

[f]Institute of Functional Nano & Soft Materials (FUNSOM), Collaborative Innovation Center of Suzhou Nano Science and Technology, Soochow University, Suzhou 215123, China

[g]University of Wisconsin Carbone Cancer Center, Madison, Wisconsin, USA 53705

Abstract

The benefits of intracellular drug delivery from nanomedicine has been limited by biological barriers and to some extent targeting capability. We investigated a size-controlled, dual tumor-mitochondria-targeted theranostic nanoplatform (Porphyrin-PEG Nanocomplexes, PPNs). The maximum tumor accumulation (15.6 %ID/g, 72 h p.i.) and ideal tumor-to-muscle ratio (16.6, 72 h p.i.) was achieved using an optimized PPN particle size of approximately 10 nm *via* PET imaging tracing. The stable coordination of PPNs with ^{177}Lu enables integration of fluorescence imaging (FL) and photodynamic therapy (PDT) with positron emission tomography (PET) imaging and internal radiotherapy (RT). Furthermore, efficient tumor and mitochondrial uptake of ^{177}Lu-PPNs greatly enhanced the efficacies of RT and/or PDT. This work developed a facile approach to fabricate tumor-targeted multi-modal nanotheranostic agents, which enables precision and radionuclide-based combination tumor therapy.

Graphical abstract

Correspondence to: Qianjun He; Xiaoli Lan; Weibo Cai.

Supporting information for this article is given via a link at the end of the document.
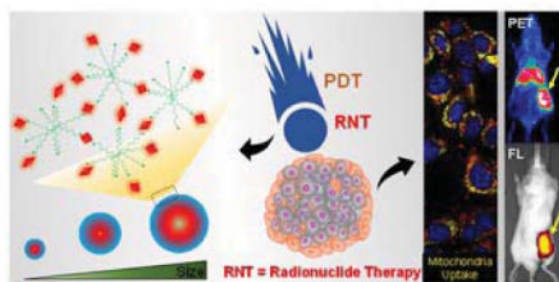
Radionuclide-based combination therapy: A dual tumor-mitochondria-targeted theranostic nanoplatform with controllable biodistribution in vivo was fabricated by complexing meso-tetra(4-carboxyphenyl)-porphyrin with 8-arm-amine-polyethylene glycol (PPNs). Efficient cancer theranostics benefit maximally from the co-location of imaging signal and radionuclide-based combination therapy component.

Keywords

Nanotheranostics; Targeted delivery; Multimodal imaging; Combined therapy; Radiotherapy

Nanomedicine is renowned for its feasibility and controllability to create 'all-in-one' multi-functional properties for cancer theranostics.[1] Nanoparticle-mediated combinatorial therapeutic regimes are increasingly being used by researchers to improve therapies due to greater tumor cell killing effects in the targeted site.[2] Specifically, radiation-based combination therapy has become a clinical standard in curative and palliative treatment regimens.[3] Recently, radionuclide therapy using particle-emitting radioisotopes (e.g., ^{177}Lu, ^{90}Y, ^{131}I) has presented promising results for the palliative treatment of several cancers.[4] Among those radionuclides, the increase in ^{177}Lu applications has enriched its potential for research and therapeutic procedures and established it at the forefront of clinical radionuclide therapy.[5] Radioisotope ^{177}Lu has favorably long nuclear decay properties ($t_{1/2}$ = 6.65 d) and is easily radiolabelled onto a variety of molecular carriers.[6] As such, ^{177}Lu promises to benefit nanoparticle-mediated combination therapy. Previous studies explored ^{177}Lu-labeled gold nanoparticles for preclinical nuclear medicine.[7] However, the clinical translation of the reported nanosystem was impeded because of high and long-term accumulation in the reticuloendothelial system (RES) and low intratumor uptake. Thus, it remains a big challenge to integrate nanocarrier tumor-targeted delivery and multi-modal imaging using ^{177}Lu to obtain a nanotheranostic with high efficacy.

Specificity of nano-theranostic reagent to cancer cells is critical for an efficient therapeutic effect with low side effects.[8] A myriad of strategies has been developed to enhance cancer targeting specificity, such as conjugation of nanomaterials with target ligands.[9] A recent report on mitochondria targeting emerged as a promising approach for cancer therapy.[10] However, there are several existing fundamental limitations on the design and synthesis of nanomaterials such as difficulties in large-scale preparation and inevitable uptake by reticuloendothelial organs.[11] Furthermore, the development of mitochondria targeting nano-theranostic reagents involves additional synthetic processes that make it much more

challenging. Therefore, the development of a nano-theranostic reagent that is easily synthesized while retaining high specificity to cancer cells would be highly desirable.

Metalloporphyrin nanoparticles have demonstrated broad utility for biomedical applications, such as in vivo imaging, diagnostics, therapeutic, and analytics.[12] In this study, a dual tumor-mitochondria-targeted theranostic nanoplatform with controllable biodistribution in vivo was fabricated by complexing meso-tetra(4-carboxyphenyl)-porphyrin (mTCPP) with 8-arm-amine-polyethylene glycol (aPEG) (PPNs). A series of PPNs with sizes of approximately 1 nm to 500 nm were synthesized by controlling the reaction time of mTCPP and aPEG. The mTCPP in the PPNs acted as a promising theranostic component based on its photodynamic therapy (PDT) properties and fluorescence imaging and was also employed to chelate radionuclide for multimodal theranostics. The chelation of PPNs with ^{64}Cu enabled the precise assessment of their biodistribution by positron emission tomography (PET) imaging. The highest tumor uptake was found to be 15.6 ± 5.7 %ID/g of PPNs-10nm while the tumor/muscle ratio was higher than 15. After the chelation of PPNs with ^{177}Lu, our results indicate that the mitochondrial uptake of ^{177}Lu-PPNs greatly enhanced the efficacies of RT and/or PDT in vitro by generating strong reactive oxygen species (ROS). This supports the promise of drug design using mitochondrial targeting for improving therapeutic outcomes because of its vital role in cell survival and susceptibility to ROS levels. Additionally, ^{177}Lu-PPNs were found to have an excellent synergistic effect using PDT and internal RT in vivo. In summary, the porphyrin-PEG nanocomplexes exhibited the following significant features: (1) A facile and robust synthesis of the nano-theranostic reagent with controllable in vivo biodistribution and a high tumor-to-muscle ratio, (2) efficient tumor and mitochondria targeting enhances the co-treatment effect of therapeutic radionuclide and PDT, and (3) cancer theranostics benefit maximally from the co-location of imaging signal and radionuclide-based combination therapy.

The synthetic reaction process of PPNs was shown in Figure 1a. As shown in Figure 1b–d and Figure S1, the color changes of PPNs were recorded and indicated that the conjugating rate of mTCPP with aPEG increased with prolonged reaction time. The DLS sizes of synthesized PPNs were 1.03 ± 0.6 nm, 10.1 ± 2.0 nm, 46.1 ± 4.0 nm, and 389.4 ± 124.8 nm, respectively. The products aggregated into a bulk gel when the reaction time reached 120 h. TEM images confirmed that the size of obtained PPNs (10 nm and 50 nm). The mTCPP of the PPNs acted as the chelate molecule for isotope labeling.[13] We found that ^{64}Cu^{2+} was immediately chelated by PPNs (Figure S2). Fluorescence imaging of ^{64}Cu-PPNs further confirmed that the nanoparticles were chelated with ^{64}Cu.

To investigate tumor uptake behaviors, mice were injected with various ^{64}Cu-PPNs. The representative maximum intensity projections (MIP) and quantitative data of PET images were shown in Figure 1e and Figure 1f. We found that ^{64}Cu-PPNs-1nm rapidly accumulated in the bladder (Figure S3). The radioactivity signal of ^{64}Cu-PPNs-1nm in the blood pool continued to decrease to 3.1 ± 1.8 %ID/g at 24 h post-injection (p.i.) (Figure 1f). The tumor-targeting efficiencies of the ^{64}Cu-PPNs-10nm were determined to be 12.5 ± 2.1 %ID/g at 24 h p.i. This was much higher than ^{64}Cu-PPNs-1nm and ^{64}Cu-PPNs-50nm, due to the enhanced permeability and retention (EPR) effect (Figure 1f). Improving the tumor-to-muscle ratio provides a larger imaging window and an increased biostability profile, which

are both important factors for clinical imaging.[14] We observed clear ^{64}Cu-PPNs accumulation in tumors compared with the surrounding muscle tissue for extended periods of time. The mean tumor-to-muscle ratios of ^{64}Cu-PPNs-1nm, ^{64}Cu-PPNs-10nm, and ^{64}Cu-PPNs-50nm were found to be 3.9 ± 2.4, 5.2 ± 2.5, and 10.4 ± 2.1, respectively at 24 h p.i. (Figure 1f). As shown in Figure S4 and S5, the final tumor uptake of ^{64}Cu-PPNs (10 nm, 50 nm) reached 15.6 ± 1.3 %ID/g (tumor-to-muscle ratios: 16.6 ± 5.7) and 7.5 ± 1.0 %ID/g (tumor-to-muscle ratios: 7.7 ± 1.1) at 72 h p.i., respectively. Previous studies have shown that the RES readily sequesters larger nanoparticles.[15] The accumulation of ^{64}Cu-PPNs in the liver remained constant over the 24 h period (Figure 1f). Considering clearance as well as liver and tumor uptake, ^{64}Cu-PPNs-10nm had a large imaging window and was the optimal choice for further investigation.

Subcellular organelle-targeted drug delivery is expected to kill cancer cells more directly and efficiently.[16] As shown in Figure 2a, the co-location of radionuclide (^{177}Lu) and PDT (mTCPP) reagent, with the targeted subcellular organelle, enhanced radionuclide-based combination therapy. Confocal microscope imaging confirmed TCPP signal of PPNs-10nm inside cells reached a saturation level after 6 h of PPNs incubation (Figure S6). ^{177}Lu was stably chelated with PPNs-10nm (Figure S7 and S8). The following in vitro assessment proved cells treated with ^{177}Lu-PPNs-10nm were more damaged than other groups (Figure 2b). No significant cytotoxicity of PPNs-10nm was observed at high concentrations. The decrease in the cell viability was also found to be dose-dependent when the amount of ^{177}Lu (20 μCi) was kept constant. Furthermore, cells treated with ^{177}Lu-PPNs and exposure to 660 nm laser were found to be damaged more than those treated with PPNs and exposure to laser only. Radionuclide therapy radiation interacts with biological substrates through direct and indirect mechanisms which involve DNA damage and overproduction of ROS, respectively.[17] We used CellROX®Green to measure intracellular ROS levels. As shown in Figure 2c, a combination of ^{177}Lu-PPNs and laser improved green fluorescence intensity, indicating much higher levels of ROS. After another 6 h of incubation, the most significant cell nucleus condensation was observed in the treatment of ^{177}Lu-PPNs with a laser as shown in Figure S9. The connection between oxidative stress and inducing mitochondrial fragmentation has been previously confirmed.[18] Here, combination treatment induced significant mitochondrial fragmentation as shown by MitoTracker Green probe (Figure S10). After staining with various subcellular organelle dyes (Figure 2d and Figure S11) selectivity for mitochondria and the nucleus, fluorescence confocal microscope images showed a clear time-dependent co-localization of PPNs in mitochondria (Figure 2e) that might be due to the slight positive surface potential of PPNs (Figure S12)

In vivo fluorescence signals from mTCPP in both ^{177}Lu-PPNs-10nm alone and co-treatment of ^{177}Lu-PPNs-10nm with laser were strong and lasted up to 14 days (Figure 3a and Figure S13a). Strong red fluorescence of tumor slices was observed in tumor sections and the vein (indicated by the arrow) verified the prominent uptake and blood circulation properties of PPNs-10nm even at 6 days p.i. (Figure 3b). During the therapy period (Figure 3c and Figure S14), ^{177}Lu-PPNs-10nm continued to accumulate in the tumor, corresponding with previous results. Ex vivo gamma camera imaging of the main organs also confirmed the radioactivity signals of both groups were primarily in the tumor (Figure S13b). In contrast, free ^{177}Lu largely accumulated in the liver and spleen (Figure S15 and Figure S16). Accumulation

of ^{177}Lu-PPNs-10nm alone and the co-treatment group in the tumor was found to be 14.8 ± 1.0 %ID/g and 15.3 ± 1.5 %ID/g, respectively (Figure 3d). After a single dose of ^{177}Lu-PPNs-10nm was injected into 4T1 tumor-bearing mice (n=3). At 72 h p.i., each tumor was exposed to a 660 nm laser as the combination therapy group. Four other groups including PBS group, mice injected with free ^{177}Lu, PPNs-10nm plus laser, and ^{177}Lu-PPNs-10nm were used as the control. Remarkably, tumor growth in combination therapy of ^{177}Lu-PPNs-10nm and laser was completely inhibited after 14 days (Figure 3e). On the contrary, neither ^{177}Lu-PPNs alone nor PPNs plus laser affected the tumor growth. Moreover, the tumors with no injection and with the injection of free ^{177}Lu grew rapidly. No noticeable toxic side effects were found in the mice based on the mice weight, serum biochemistry analysis, and H&E staining (Figure 3f, Figure S17, and S18).

In summary, a nanotheranostic agent with controllable biodistribution in vivo and subcellular organelle targeting in vitro was facilely fabricated. Notably, the PPNs were found to bind selectively to mitochondria and exhibited excellent synergistic effects after chelating with ^{177}Lu in the co-treatment of ^{177}Lu-PPNs and laser. Furthermore, in vivo co-treatment of ^{177}Lu-PPNs and PDT demonstrated excellent tumor accumulation and powerful therapeutic efficacy.

Supplementary Material

Refer to Web version on PubMed Central for supplementary material.

Acknowledgments

References

1. Shi J, Kantoff PW, Wooster R, Farokhzad OC. Nat Rev Cancer. 2017; 17:20–37. [PubMed: 27834398]

2. Goel S, Ni D, Cai W. ACS Nano. 2017; 11:5233–5237. [PubMed: 28621524]

3. a) Mi Y, Shao Z, Vang J, Kaidar-Person O, Wang AZ. Cancer Nanotechnol. 2016; 7:016–0024.b) Hirayama R. Igaku Butsuri. 2014; 34:65–69. [PubMed: 25693293]

4. Banerjee S, Pillai MR, Knapp FF. Chem Rev. 2015; 115:2934–2974. [PubMed: 25865818]

5. a) Dash A, Pillai MR, Knapp FF Jr. Nucl Med Mol Imaging. 2015; 49:85–107. [PubMed: 26085854] b) Reber J, Haller S, Leamon CP, Muller C. Mol Cancer Ther. 2013; 12:2436–2445. [PubMed: 24030631]

6. Shultz MD, Duchamp JC, Wilson JD, Shu CY, Ge J, Zhang J, Gibson HW, Fillmore HL, Hirsch JI, Dorn HC, Fatouros PP. J Am Chem Soc. 2010; 132:4980–4981. [PubMed: 20307100]

7. Vilchis-Juarez A, Ferro-Flores G, Santos-Cuevas C, Morales-Avila E, Ocampo-Garcia B, Diaz-Nieto L, Luna-Gutierrez M, Jimenez-Mancilla N, Pedraza-Lopez M, Gomez-Olivan L. J Biomed Nanotechnol. 2014; 10:393–404. [PubMed: 24730235]

8. Pan L, He Q, Liu J, Chen Y, Ma M, Zhang L, Shi J. J Am Chem Soc. 2012; 134:5722–5725. [PubMed: 22420312]

9. Kamaly N, Xiao Z, Valencia PM, Radovic-Moreno AF, Farokhzad OC. Chem Soc Rev. 2012; 41:2971–3010. [PubMed: 22388185]

10. Chakrabortty S, Agrawalla BK, Stumper A, Vegi NM, Fischer S, Reichardt C, Kogler M, Dietzek B, Feuring-Buske M, Buske C, Rau S, Weil T. J Am Chem Soc. 2017; 139:2512–2519. [PubMed: 28097863]

11. a) Sanhai WR, Sakamoto JH, Canady R, Ferrari M. Nat Nanotechnol. 2008; 3:242–244. [PubMed: 18654511] b) Hare JI, Lammers T, Ashford MB, Puri S, Storm G, Barry ST. Adv Drug Deliv Rev. 2017; 108:25–38. [PubMed: 27137110]

12. Shao S, Rajendiran V, Lovell JF. Coordi Chem Rev.

13. Cheng L, Kamkaew A, Sun H, Jiang D, Valdovinos HF, Gong H, England CG, Goel S, Barnhart TE, Cai W. ACS Nano. 2016; 10:7721–7730. [PubMed: 27459277]

14. a) Olson ES, Jiang T, Aguilera TA, Nguyen QT, Ellies LG, Scadeng M, Tsien RY. Proc Natl Acad Sci U S A. 2010; 107:4311–4316. [PubMed: 20160077] b) Wan W, Guo N, Pan D, Yu C, Weng Y, Luo S, Ding H, Xu Y, Wang L, Lang L, Xie Q, Yang M, Chen X. J Nucl Med. 2013; 54:691–698. [PubMed: 23554506]

15. a) Liu J, Yu M, Zhou C, Yang S, Ning X, Zheng J. J Am Chem Soc. 2013; 135:4978–4981. [PubMed: 23506476] b) Xu J, Yu M, Carter P, Hernandez E, Dang A, Kapur P, Hsieh JT, Zheng J. Angew Chem Int Ed. 2017; 56:13356–13360.Angew Chem. 2017; 129:13541–13545.

16. Peng H, Tang J, Zheng R, Guo G, Dong A, Wang Y, Yang W. Adv Healthc Mater. 2017; 6:27.

17. Pouget JP, Lozza C, Deshayes E, Boudousq V, Navarro-Teulon I. Front Med (Lausanne). 2015; 2:12. [PubMed: 25853132]

18. a) Sastre J, Pallardo FV, Vina J. IUBMB Life. 2000; 49:427–435. [PubMed: 10902575] b) Sastre J, Pallardó FV, García de la Asunción J, Viña J. Free Radical Res. 2000; 32:189–198. [PubMed: 10730818]
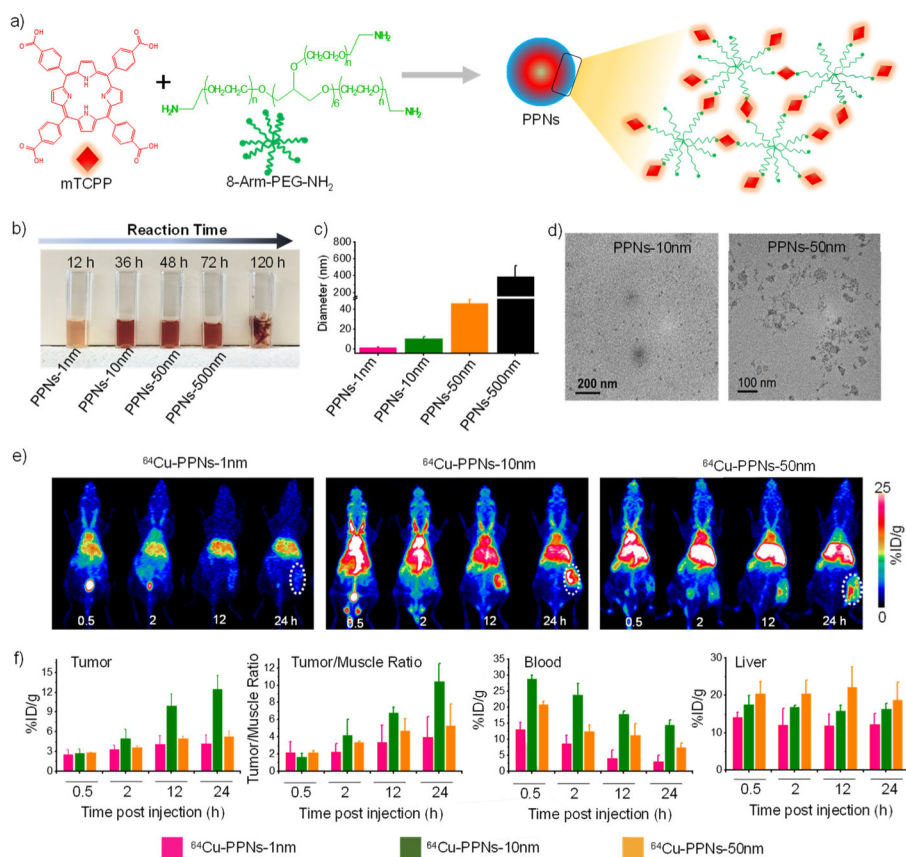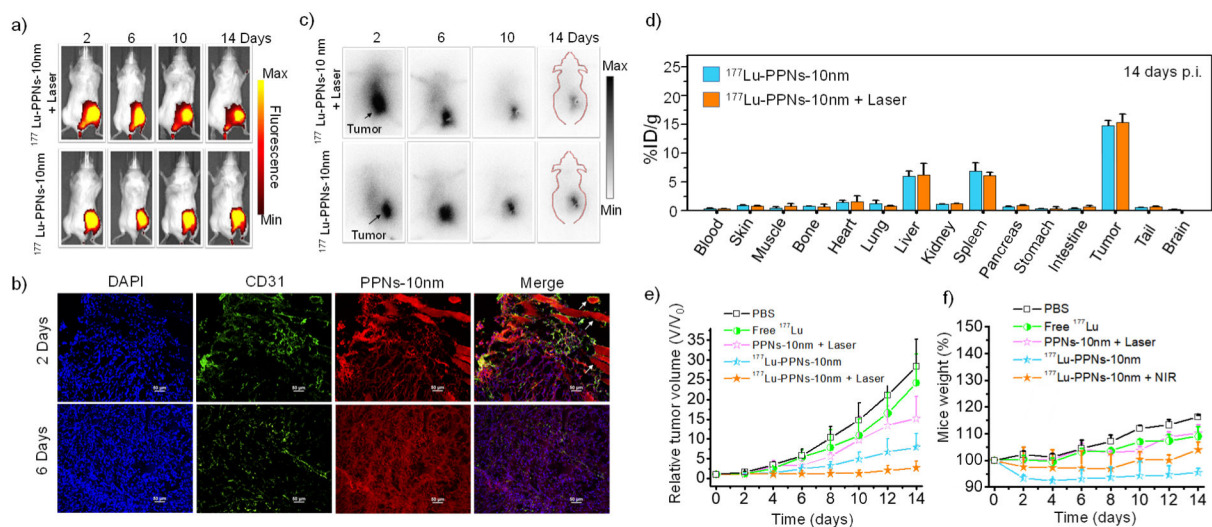
Figure 1.
a) A synthetic scheme of the mTCPP-aPEG nanocomplexes (PPNs). b) Photo and c) DLS diameter of obtained PPNs. d) TEM images of PPNs of approximately 10 nm (left) and 50 nm (right). e) Maximum intensity projections of PET imaging of tumor-bearing mice after injection of ^{64}Cu-PPNs. f) Quantitative biodistribution obtained from ROI analysis of PET images.
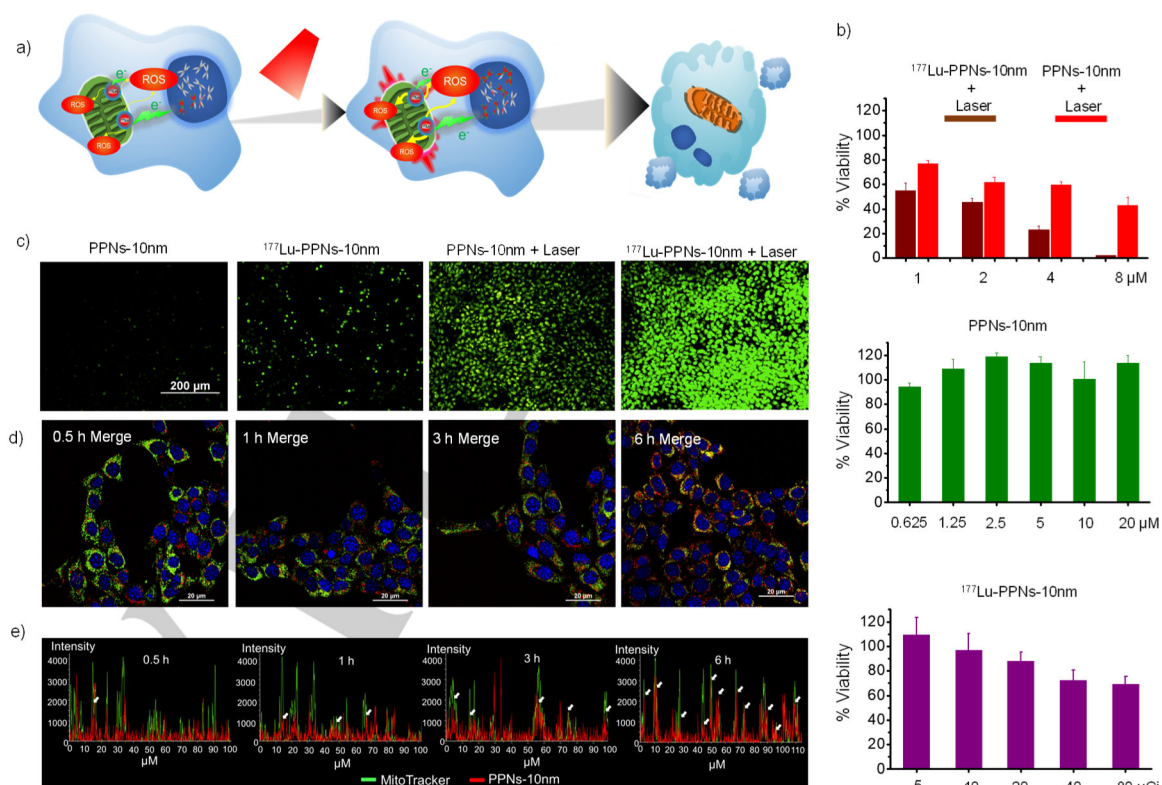
Figure 2.
a) A schematic illustration of the combination of PDT and RNT using ^{177}Lu-PPNs-10nm.
First, ^{177}Lu-PPNs-10nm were introduced into the cells. After PPNs attached to
mitochondria, the cells were exposed to 660 nm laser. The co-location of radionuclide and
PDT reagent with the targeting subcellular organelle enhanced the radionuclide-based
combination therapy. b) Cell viability of 4T1 cells treated with various concentrations of
PPNs-10nm and ^{177}Lu-PPNs-10nm with or without laser (660 nm). c) Measurement of the
intracellular ROS levels by CellROX®Green. d) Confocal microscopy images of 4T1 cells
incubated with PPNs and treated with commercial organelle trackers (Blue: Hoechst 33342;
Green: MitoTracker® Green FM; Red: PPNs-10nm). e) Co-location analysis of PPNs-10nm
and MitoTracker® Green FM. The white arrow indicated the overlay of PPNs-10nm and
mitochondria.

Figure 3.

a) In vivo fluorescence images of 4T1 tumor-bearing mice taken after post-injection of ^{177}Lu-PPNs-10nm. b) Confocal images of tumor tissues after injection of PPNs-10nm. (scale bar 50 μm). c) Corresponding gamma camera images of mice. d) Biodistribution of ^{177}Lu-PPNs-10nm alone and cotreatment of ^{177}Lu-PPNs-10nm and laser. e) Tumor sizes and f) mouse weight after each treatment (n=3).